Topological insulating phases from two-dimensional nodal loop semimetals

Linhu Li[1,2] and Miguel A. N. Araújo[1,2,3]
[1]*Beijing Computational Science Research Center, Beijing 100089, China*
[2]*CeFEMA, Instituto Superior Técnico, Universidade de Lisboa, Avenida Rovisco Pais, 1049-001 Lisboa, Portugal*
[3]*Departamento de Física, Universidade de Évora, P-7000-671 Évora, Portugal*
(Received 1 August 2016; published 10 October 2016)

Starting from a minimal model for a two-dimensional nodal loop semimetal, we study the effect of chiral mass gap terms. The resulting Dirac loop anomalous Hall insulator's Chern number is the phase-winding number of the mass gap terms on the loop. We provide simple lattice models, analyze the topological phases, and generalize a previous index characterizing topological transitions. The responses of the Dirac loop anomalous Hall and quantum spin Hall insulators to a magnetic field's vector potential are also studied both in weak- and strong-field regimes, as well as the edge states in a ribbon geometry.

DOI: 10.1103/PhysRevB.94.165117

I. INTRODUCTION

The nontrivial topological properties of fermions, which have attracted great attention recently, stem from their low-energy Dirac-like band dispersion and its associated chiralities. Differently from conventional physical phases, topological phases are classified by discrete topological invariants of occupied bands, rather than continuous order parameters [1,2]. Depending on its time-reversal, particle-hole, and chiral symmetries, a gapped system, i.e., insulator or superconductor, can be classified into ten topological classes, five of which can support topologically nontrivial phases depending on the dimension of the system [3]. In an insulating system, the bulk gap contains nontrivial boundary states whose chirality or helicity is determined by the topological invariants. In superconductors, the possibility of realizing Majorana fermions has spurred intense research because of their potential application in quantum computation [4].

In some three-dimensional systems, there may also be linear band touching at discrete Dirac or Weyl points, or "nodes," in the Brillouin zone (BZ). Dirac and Weyl semimetals have been the focus of intense research [5–9], as they are gapless systems which can exhibit topological properties. A Dirac semimetal enjoys both time-reversal and inversion symmetries. When one of these symmetries is broken, Weyl nodes with opposite chiralities separated in momentum space may appear and the semimetal exhibits surface Fermi arcs and the chiral anomaly [10]. Examples of Dirac semimetals are Na_3Bi and Cd_3As_2 [11–17]. The Weyl semimetal state has been experimentally confirmed in the TaAs family [18–22].

More recently, a new class of three-dimensional semimetal with nodal lines has attracted growing interest [23–25], following the suggestion for its realization in the hyperhoneycomb lattice [23]. In this case, the linear band touching occurs along a closed loop in the BZ. The concept of nodal loop semimetal is relatively new and awaits further investigation.

In addition to the above types of three-dimensional topological semimetals (Dirac, Weyl, and nodal line), a more recent proposal for the concept of a *two-dimensional nodal line* semimetal has emerged and a suggestion for its physical realization in a new composite lattice composed of interpenetrating kagome and honeycomb lattices has been presented [26]. Spin-orbit coupling can open a small gap at the node line, resulting in a novel topological crystalline insulator.

Motivated by these recent developments, here we study the nodal loop (NL) semimetal in two dimensions, for spinless fermions. The introduction of mass gap terms may lead to topological insulating phases. We derive an expression for the Chern number of the resulting Dirac loop anomalous Hall insulator (DLAHI). The Chern number is equivalent to the winding number of the mass terms' phase along the loop and can be regarded as the loop's chirality. We examine the topological transitions that take place as model parameters change and generalize a previous index that characterizes such transitions. The effect of a magnetic field on a DLAHI is also studied and compared to the case of Dirac point systems.

In Sec. II, we introduce the minimal model for a NL semimetal, consider a mass gap, and study the topological properties of the DLAHI. Section III is devoted to the study of magnetic field effects. In Sec. IV, we summarize our results and make some concluding remarks.

II. TOPOLOGICAL INSULATOR IN GENERALIZED 2D NODAL LOOP SEMIMETAL

A. Minimal model and topological invariant

To model a nodal loop semimetal in two dimensions (2D), it is necessary for the system to have at least two bands, and the Hamiltonian can be written as

$$H = \boldsymbol{h}(\boldsymbol{k}) \cdot \boldsymbol{\tau}, \tag{1}$$

where τ_α ($\alpha = 1,2,3$) are the Pauli matrices acting on sublattice ("pseudospin") space and the Bloch wave vector $\boldsymbol{k} = (k_x, k_y)$ runs over the Brillouin zone (BZ). We first consider a minimal Hamiltonian with a nodal circular loop [24],

$$h_3 = \hbar v_0 (k - k_0). \tag{2}$$

Here, $k = \sqrt{k_x^2 + k_y^2}$ and k_0 is the loop radius. Equation (2) is supposed to be a valid approximation in the region $k \approx k_0$ of the BZ. This Hamiltonian gives a NL semimetal where the valence and conduction bands cross at $k = k_0$ if $h_1 = h_2 = 0$. In a doped system, the Fermi surface would be a ring with radius k_0, but we shall not consider doped systems below. h_1 and h_2 can be viewed as two independent mass terms. Nonzero h_1 and h_2 may open a gap and turn the system into an insulator if only the lower (valence) band is occupied. We take the band gap $\Delta \equiv \sqrt{h_1^2 + h_2^2} \ll \hbar v_0 k_0$. It may take on a constant value on the

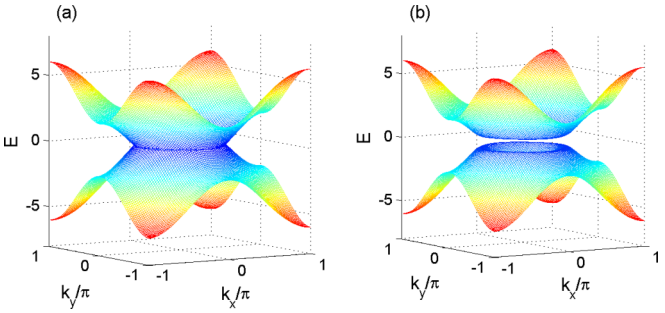

FIG. 1. (a) The dispersion relation of a NL semimetal. (b) The gapped spectrum.

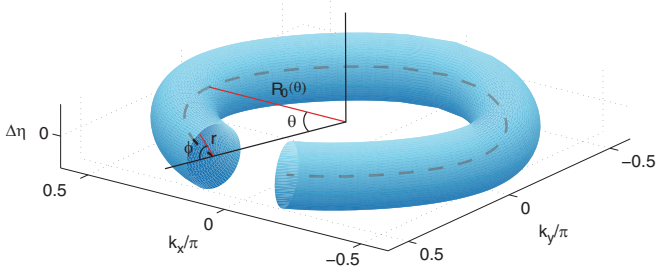

FIG. 2. The torus in Eq. (9) in the parameter space ($\mathbf{k}, \Delta\eta \equiv \eta - \eta_0$). The dashed line is the nodal loop when $\eta_0 = 0$. The flux of $\boldsymbol{V}$ though the torus surface gives the index C_l.

loop or have some $\boldsymbol{k}$ dependence. A plot of the dispersion is shown in Fig. 1.

The topological properties of this model can be characterized by the Chern number C of the occupied band, which is defined as

$$C = \frac{1}{2\pi}\int V_{\boldsymbol{k}} dk_x dk_y, \tag{3}$$

$$V_{\boldsymbol{k}} = \partial_{k_x} A_{k_y} - \partial_{k_y} A_{k_x}, \tag{4}$$

where $V_{\boldsymbol{k}}$ is the Berry curvature and $A_\alpha = i\langle\varphi(\boldsymbol{k})|\partial_\alpha|\varphi(\boldsymbol{k})\rangle$ is the Berry connection [27], $\varphi(\boldsymbol{k})$ is a Bloch eigenstate of the occupied band, and the integral is over the two-dimensional Brillouin zone. Equation (4) yields a well-defined result provided that the loop is gapped.

We shall now show that a simple expression for C can be obtained which involves only the circulation of the phase of $h_1 - ih_2$ along the loop. For the two-band system described by Eq. (1), the Berry curvature of the lower band takes on the familiar form,

$$V_{\boldsymbol{k}} = \frac{1}{2|\boldsymbol{h}|^3}\frac{\partial \boldsymbol{h}}{\partial k_x}\times\frac{\partial \boldsymbol{h}}{\partial k_y}\cdot\boldsymbol{h}, \tag{5}$$

where $|\boldsymbol{h}|=\sqrt{h_1^2+h_2^2+h_3^2}$. Using polar coordinates in momentum space, (k,θ), we write $(k_x,k_y) = k(\cos\theta, \sin\theta)$. We rewrite the Berry curvature in polar coordinates and, considering that the contribution to the integral (3) comes from the vicinity of the loop where Eq. (2) holds, we obtain

$$C = \frac{\hbar v_0}{4\pi}\int \frac{dk d\theta}{|\boldsymbol{h}|^3}(h_2\partial_\theta h_1 - h_1\partial_\theta h_2). \tag{6}$$

The integration over k can be performed under the assumption that the gap $\Delta \ll \hbar v_0 k_0$. This allows us to extend the integration limits of k to the whole real axis and obtain

$$C = \mathrm{sgn}(v_0)\int_0^{2\pi}\frac{d\theta}{2\pi}\frac{h_2\partial_\theta h_1 - h_1\partial_\theta h_2}{h_1^2+h_2^2}, \tag{7}$$

where the integration is performed on the loop $h_3 = 0$. The expression (7) is just the winding number for the phase of $h_1 - ih_2$. The above derivation may be regarded as an extension of the contribution from a single Dirac point to the Chern number [28], which can be $\pm 1/2$. By analogy, Eq. (7) assigns a chirality to the gapped loop. While a fermionic system must have an even number of Dirac points [29], there may be only one, or an arbitrary number of, NLs.

The above Chern number is ill defined when the gap closes, $h_1 = h_2 = 0$, as the integrand of Eq. (7) diverges. At a topological phase transition, the gap closes and a definition of a $\mathbb{Z}$ index characterizing the transition can be achieved in the extended three-dimensional parameter space, $(\boldsymbol{k},\eta)$, where η is a transition driving parameter [30]. We assume the system to be an insulator for general η and the gap closes at $\eta = \eta_0$. If the gap closes at one or more discrete points in the BZ, a topological number C_p can be calculated as the flux of the Berry curvature through a sphere $\boldsymbol{S}$ enclosing each of these points in the parameter space of $(\boldsymbol{k},\eta)$,

$$C_p = \frac{1}{2\pi}\oiint \boldsymbol{V}\cdot d\boldsymbol{S}, \tag{8}$$

where $\boldsymbol{V} = \nabla\times i\langle\varphi(\boldsymbol{k},\eta)|\nabla|\varphi(\boldsymbol{k},\eta)\rangle$ is the Berry curvature in the extended parameter space. The summation of C_p over every gap closing point gives the change of the Chern number C across the transition [30].

We can extend the above index to the case of a nodal loop semimetal by defining a similar index, C_l, as the Berry curvature flux through a torus enclosing the loop. In the parameter space of $\boldsymbol{k}$ and η, this torus can be written as

$$\begin{aligned} k_x &= [k_0 + r\cos\phi]\cos\theta, \\ k_y &= [k_0 + r\cos\phi]\sin\theta, \\ \eta &= \eta_0 + r\sin\phi, \end{aligned} \tag{9}$$

where ϕ is a new angular parameter on the torus and r is the tube radius, as shown in Fig. 2. We may recast the surface integral in Eq. (8) using Eqs. (9) and θ,ϕ as integration variables, as

$$C_l = \frac{1}{2\pi}\iint V_{\phi,\theta} d\phi d\theta,$$

$$V_{\phi,\theta} = \partial_\phi A_\theta - \partial_\theta A_\phi. \tag{10}$$

The value of C_l is independent of r as long as no gap closing point exists other than the nodal loop within the torus. This index C_l can serve as a topological invariant, which gives the change of Chern number C at a transition where $\eta = \eta_0$.

B. Specific models

We now provide some specific lattice models to illustrate the topological phases of a 2D nodal loop. Note that in a lattice model, the nodal loop is not a perfect circle in the BZ, so the loop radius k_0 is actually a function of the polar coordinate

θ, $k_0 = k_0(\theta)$. Chern numbers for these lattice models are calculated numerically with the method described in Ref. [31]. Following this technique, the parameter space (k_x, k_y), or (θ, ϕ) for the calculation of C_l, is discretized and the circulations of the Berry connection on small plaquettes are performed.

We first consider the following model for the vector $\boldsymbol{h}(\boldsymbol{k})$ in Eq. (1):

$$\begin{aligned} h_1(\boldsymbol{k}) &= \lambda \sin k_y + M, \\ h_2(\boldsymbol{k}) &= -\lambda \sin k_x, \\ h_3(\boldsymbol{k}) &= \mu - 2(\cos k_x + \cos k_y). \end{aligned} \tag{11}$$

The condition $h_3 = 0$ gives a nodal loop around the origin for $0 < \mu < 4$, or around the point (π, π) for $-4 < \mu < 0$. We shall take $\mu = 2$ below. When $M = 0$, this model is also known as the Qi-Wu-Zhang model for spin-1/2 systems [32]. The term M couples two pseudospin components at the same lattice site.

Model (11), for $4 > \mu > 0$, has two different topological phases with $C = 0$ or $C = -1$. In Fig. 3(a), we show the phase diagram with $\mu = 2$. The topological phase boundary is given by $|\lambda| = M$, where the gap closes at a single point $\boldsymbol{k} = [0, -\mathrm{sgn}(\lambda \cdot M)\pi/2]$, except in the case $\lambda = M = 0$, where the system is a nodal loop semimetal. In Figs. 3(b)–3(g), we plot $[h_1(\theta), -h_2(\theta)]$ for $h_3 = 0$, with θ varying from 0 to 2π, for different parameter choices. The Chern number $C = -1$ when $h_1 - ih_2$ winds clockwise around the origin, in accordance with Eq. (7).

We now study the topological transitions that take place as the parameters λ and M change, either independently or along a chosen curve in the (λ, M) plane. We start by examining two cases where the spectral gap closes over the whole loop, at the transition. A case where $M = 0$ and λ varies is plotted as a red dashed line in Fig. 3(a). Going along such a trajectory, no topological phase transition exists, as $C = -1$ always. Now consider the case where $M = \lambda(1 - \lambda)$, which is plotted as the red curve in Fig. 3(a): a transition between $C = 0$ and $C = -1$ phases occurs at $M = \lambda = 0$. We use Eq. (10) to calculate the index C_l, where we identify the driving parameter η with λ and take the torus inner radius $r = 10^{-4}$ in Eq. (9). Equation (10) then gives $C_l = 0$ and $C_l = -1$ for these two cases, respectively, which indicates the change of C at the transition point.

In Figs. 3(b)–3(d), we show how the winding path $[h_1(\theta), -h_2(\theta)]$ evolves for a topological phase transition where the gap closes at only one point on the loop, and the system evolves from $C = 0$ to $C = -1$. For this case, Eq. (8) gives $C_p = -\mathrm{sgn}(\lambda \cdot M)$, as expected. Similarly, Figs. 3(e)–3(g) show the winding paths of $h_1 - ih_2$ as the model evolves with $-0.2 \leqslant \lambda \leqslant 0.2$ and $M = \lambda(1 - \lambda)$. For this case, we obtain $C_l = -1$. Note that Figs. 3(c) and 3(f) show winding paths for two gapless spectra: Fig. 3(c) shows the situation where the gap closes at only one point of the loop, and Fig. 3(f) depicts the case where the gap vanishes over the whole loop.

In the above lattice model, the Chern number may only be ± 1 or 0, as the winding path may go around the origin no more than once. However, if the mass terms h_1 and h_2 contain higher harmonics, the winding path will be more complicated and the system may have higher Chern number phases. As an

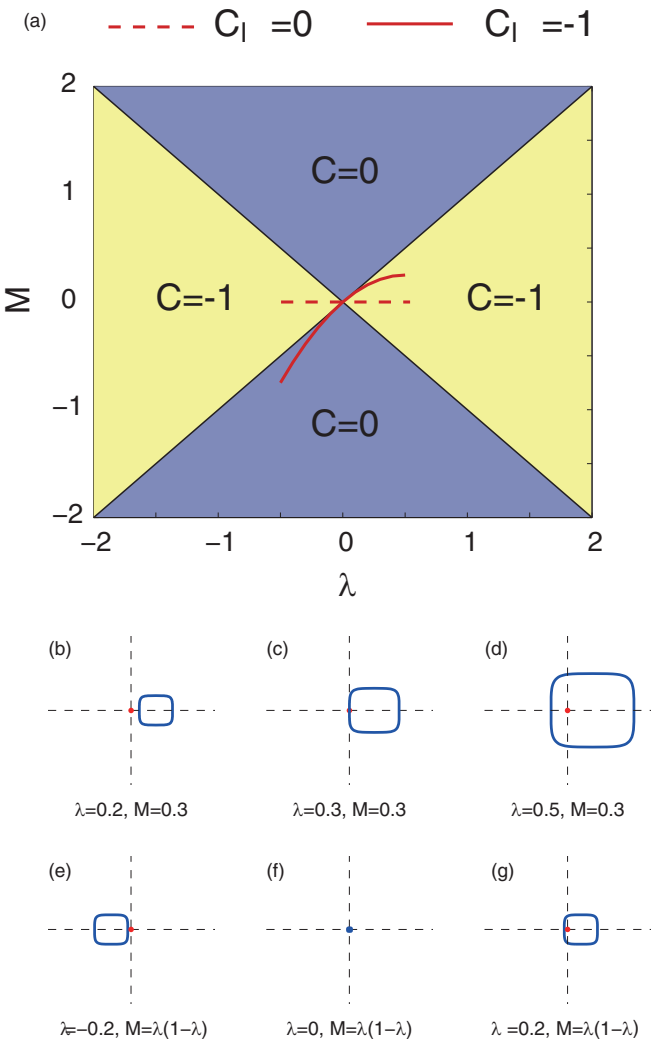

FIG. 3. (a) The phase diagram of model (11). The red and dashed lines are trajectories along which C_l is calculated, as explained in the text. (b)–(g) Winding paths, $[h_1(\theta), -h_2(\theta)]$, as $0 \leqslant \theta < 2\pi$ and $h_3 = 0$. The direction of the winding path is clockwise for each case, yielding $C = -1$ when it encloses the origin, according to Eq. (7).

example, we can choose the vector $\boldsymbol{h}(\boldsymbol{k})$ as

$$\begin{aligned} h_1(\boldsymbol{k}) &= \lambda \sin(2k_y) + M, \\ h_2(\boldsymbol{k}) &= -\lambda \sin(2k_x), \\ h_3(\boldsymbol{k}) &= \mu - 2(\cos k_x + \cos k_y). \end{aligned} \tag{12}$$

In Fig. 4, we plot $[h_1(\theta), -h_2(\theta)]$ for different parameter choices together with the corresponding Chern numbers. Figures 4(a)– 4(c) illustrate how μ changes the shape of the winding paths, and Figs. 4(d)– 4(f) show how M changes the position of the winding path relative to the origin. λ will change the size of the path (not shown in the figures).

In the recent proposal [26] for the realization of the 2D nodal loop system in a kagome-honeycomb mixed lattice, spin-orbit terms were shown to introduce mass gap terms with d_{xy} and $d_{x^2-y^2}$ symmetry. The system considered is time-reversal invariant and such terms yield $C = \pm 2$ in two effectively decoupled subspaces.

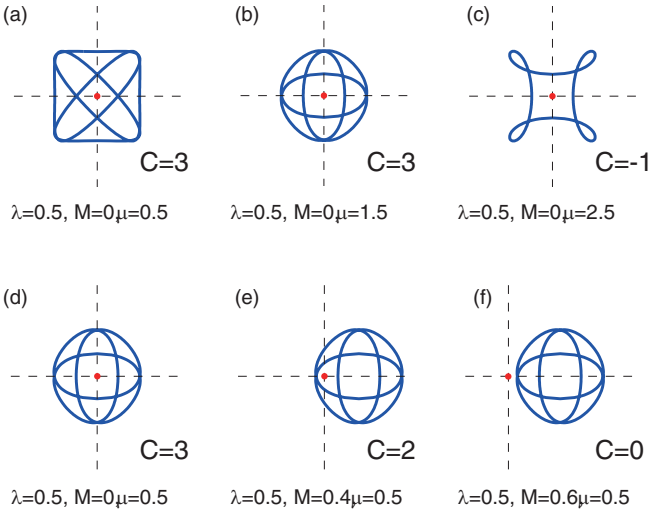

FIG. 4. Winding paths $[h_1(\theta), -h_2(\theta)]$ for model (12) for different parameter choices. The direction of the winding path is counterclockwise except in (c), where it is clockwise.

III. MAGNETIC FIELD

We now take the nodal loop Hamiltonian (1)–(13) as a model for spinless fermions on a lattice and analyze the effect of a magnetic field's vector potential.

In the case of the anomalous Hall insulator with Dirac points, it has been shown that a weak field turns the system into a metal with half-filled Landau levels (LLs) [28,33–35], while a topologically trivial insulator remains insulating under the field.

In order to understand the effect of a weak magnetic field on a NL, we follow the same procedure as in Ref. [28] and introduce a vector potential $\boldsymbol{A}$, which minimally couples to the orbital degrees of freedom, $-i\hbar\nabla \to -i\hbar\nabla - e\boldsymbol{A}$, where $e<0$ denotes the electron charge. It is convenient to replace Eq. (2) with

$$h_3 = \hbar^2\frac{k^2-k_0^2}{2m}, \tag{13}$$

which, when linearized, yields Eq. (2). We rewrite (13) in real space as

$$h_3 = -\hbar^2\frac{\partial_x^2+\partial_y^2+k_0^2}{2m}. \tag{14}$$

If we further choose constant $h_{1(2)}$ with $\sqrt{h_1^2+h_2^2}\equiv\Delta\ll\frac{\hbar^2k_0^2}{2m}$, then the NL becomes gapped and is a topologically trivial insulator at half filling. We write $\boldsymbol{A}=B(0,x,0)$ and the wave functions as

$$\psi_{\kappa,n} = e^{i\kappa y}\phi_n\left(x-\frac{\hbar\kappa}{eB}\right)\cdot\begin{pmatrix}\alpha\\ \beta\end{pmatrix}. \tag{15}$$

Here, $n=0,1,\ldots$ denotes the LL index, $\omega_c=|eB|/m$ denotes the cyclotron frequency, and $\phi_n(x)$ is a harmonic-oscillator wave function. The column vector $(\alpha,\beta)^T$ solves the eigenproblem,

$$\left\{\left[\left(n+\frac{1}{2}\right)\hbar\omega_c-\frac{(\hbar k_0)^2}{2m}\right]\tau_3+h_1\tau_1+h_2\tau_2\right\}\begin{pmatrix}\alpha\\ \beta\end{pmatrix} = E_n\begin{pmatrix}\alpha\\ \beta\end{pmatrix}, \tag{16}$$

and the energy levels are given by

$$E_n = \pm\sqrt{\left[\left(n+\frac{1}{2}\right)\hbar\omega_c-\frac{(\hbar k_0)^2}{2m}\right]^2+\Delta^2}. \tag{17}$$

The lowest LL ($n=0$) is far from the Fermi level if $\hbar\omega_c \ll (\hbar k_0)^2/(2m)$. At half filling, the lower-branch LLs are fully occupied and the ones close to the Fermi level have high index $n=N$ such that $(N+1/2)\hbar\omega_c \approx (\hbar k_0)^2/(2m)$.

The charge Hall conductance σ_{yx} takes on quantized values between the LLs. Each filled LL contributes e^2/h to σ_{yx}. In the loop gap, $\sigma_{yx}=0$.

Because high-order LLs are close to the Fermi level, one may consider the semiclassical dynamics in the magnetic field. The semiclassical motion is determined by the equations

$$\hbar\dot{\boldsymbol{k}} = ev_{\boldsymbol{k}}\times\boldsymbol{B},\quad \dot{\boldsymbol{r}} = v_{\boldsymbol{k}}, \tag{18}$$

where the group velocity $v_{\boldsymbol{k}}$ in the upper/lower band obeys $\hbar v_{\boldsymbol{k}} = \pm\partial|\boldsymbol{h}|/\partial\boldsymbol{k}$. Within this approach, the electrons follow orbits in the (k_x,k_y) plane determined by the Bohr-Sommerfeld quantization rule. Equations (18) cannot be directly applied to the gapped loop Hamiltonian, however. Instead, they may be applied to either branch of the massless loop in Eq. (14) with $h_1=h_2=0$. If we take $B>0$, for instance, then the electron orbits in $\boldsymbol{k}$ space go counterclockwise for the lower branch, while they go clockwise in the upper branch. The mass terms $h_{1(2)}$ cause quantum mixing of the orbits of both branches, as Eq. (16) explicitly shows. As we go up in energy, we lose clockwise and gain counterclockwise orbits, hence the Hall conductance increases.

Considering now the case of a topological system, we take $h_1=\hbar vk_y, h_2=-\hbar vk_x$, and h_3 from Eq. (14). Then the gap on the loop is $\Delta=\hbar vk_0 \ll (\hbar k_0)^2/(2m)$. The Chern number of the lower band is $C=-1$. It is convenient to define the operator $\hat{\mathcal{O}}=ip_x+\hbar\kappa-eBx$, which obeys the commutation relation $[\hat{\mathcal{O}},\hat{\mathcal{O}}^\dagger]=-2\hbar eB$. The Hamiltonian now takes the form

$$\hat{H} = \begin{pmatrix}\frac{\hat{\mathcal{O}}^\dagger\hat{\mathcal{O}}-\hbar eB-(\hbar k_0)^2}{2m} & v\hat{\mathcal{O}}\\ v\hat{\mathcal{O}}^\dagger & -\frac{\hat{\mathcal{O}}^\dagger\hat{\mathcal{O}}-\hbar eB-(\hbar k_0)^2}{2m}\end{pmatrix}. \tag{19}$$

The eigenstates for $B>0$ involve the same set of harmonic-oscillator functions ϕ_n above,

$$\psi_{\kappa,n} = e^{i\kappa y}\begin{pmatrix}\alpha\phi_n\\ \beta\phi_{n+1}\end{pmatrix},\quad n\geqslant 0, \tag{20}$$

with energy

$$E_n = -\frac{\hbar\omega_c}{2} \pm\sqrt{\left[\left(n+\frac{1}{2}\right)\hbar\omega_c-\frac{(\hbar k_0)^2}{2m}\right]^2+2(n+1)\hbar\omega_c mv^2}. \tag{21}$$

Additionally, there is also the "0-LL" state,

$$\psi_0 = e^{i\kappa y}\begin{pmatrix} 0 \\ \phi_0 \end{pmatrix}, \tag{22}$$

$$\bar{E}_0 = \frac{(\hbar k_0)^2}{2m} - \frac{\hbar\omega_c}{2}. \tag{23}$$

This eigenstate lies high above the Fermi level and is, therefore, empty.

We thus find that the spectrum contains an odd number of LLs: the Fermi level for the half-filled system is a half-filled LL with high index $n = N$ that minimizes the square root in Eq. (21) and with energy above the loop gap,

$$E_N \approx -\frac{\hbar\omega_c}{2} + \Delta, \tag{24}$$

and $\alpha \approx \beta$ in expression (20).

Had we chosen a Hamiltonian with opposite chirality, hence $C = 1$, the 0-LL state would live on the other sublattice and have energy symmetric to that in Eq. (23). So, it would be occupied. The Fermi level would sit *below* the loop gap, $E_N \approx \frac{\hbar\omega_c}{2} - \Delta$, which would be half filled. Therefore, the position of the Fermi LL with respect to the gap is the same as in the single Dirac cone problem [28],

$$E_N \approx \left(\frac{\hbar\omega_c}{2} - \Delta\right)\mathrm{sgn}(C \cdot B). \tag{25}$$

However, unlike the Dirac cone problem, where one has to consider at least two cones because of the fermion doubling theorem [29], here we may have only one nodal loop in the BZ and get an odd number of LLs.

As before, each filled LL contributes e^2/h to the charge Hall conductance, σ_{yx}. The existence of the 0-LL either above or below the loop gap, depending on the nodal loop's chirality, determines the Hall conductance in the gap. If $C = \pm 1$, the 0-LL lies below/above and $\sigma_{yx} = \pm e^2/h$ in the gap.

Endowing the electrons with spin, the simplest topological insulator [36] with a Dirac loop gap and conserved s_z could have a $C = 1$ Hamiltonian for up-spin electron and $C = -1$ for down spin. The Chern matrix [37] would be diagonal with $C_\uparrow = -C_\downarrow = 1$. The spin Chern number [37] $C_{sc} = C_\uparrow - C_\downarrow = 2C$, with $\nu = (C_{sc} \mathrm{mod} 4)/2$ [38,39]. The magnetic field breaks time-reversal symmetry (TRS), restoring the $\mathbb{Z}$ index C, which counts the number of edge states for each spin projection running in a given edge. In thermal equilibrium, the electrons migrate to the E_N level sitting below the gap, given by Eq. (23), so the system becomes spin polarized with spin density $|eB|/h$. This is because the spin-↑ electrons fill up their 0-LL, while the spin-↓ electrons have it empty. This spin density is half of that for two Dirac points, discussed in Ref. [28]. Note that the spin polarization is achieved without considering the Zeeman coupling to spin. The charge Hall conductance $\sigma_{yx} = 0$ because the two subsystems' contributions cancel. The spin Hall conductance $\sigma^z_{yx} = e/(2\pi)$, however. Such a state is a spin Hall insulator with magnetization and it is stable against potential disorder, but unstable against spin-flip perturbations, in which case it would become a trivial insulator.

At stronger magnetic field, the magnetic length becomes comparable to the lattice spacing and the energy spectrum exhibits the fractal structure known as the Hofstadter butterfly [40]. A calculation of Hofstadter butterfly spectra for Weyl nodes in 3D systems has recently been done [41]. Figure 5 shows the Hofstadter spectrum for the model (11) with $\mu = 2$, $\lambda = -0.1$, and $M = 0$, at half filling. The Fermi energy lies above the gap, for small flux, as the model's Chern number $C = -1$, in agreement with the above discussion. Quantized Hall conductances (in units of e^2/h) are also shown in some of the Hofstadter gaps. Although the half-filled system is metallic for small field, it may become an insulator with zero Hall conductance at higher flux values.

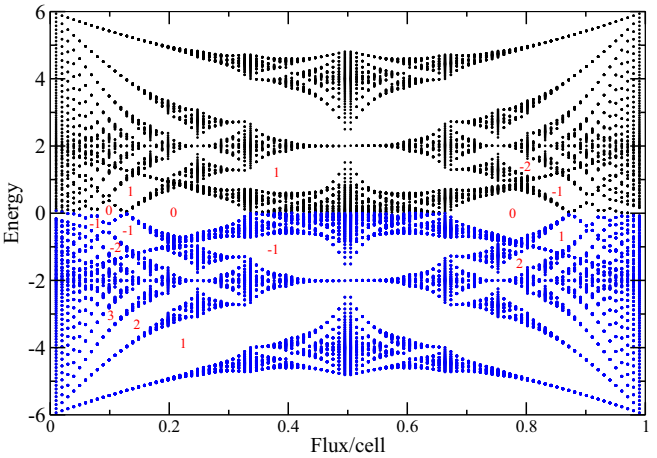

FIG. 5. Weyl loop Hofstadter spectrum of model (11), which has $C = -1$ at zero field. The flux per lattice cell is expressed in units of the flux quantum, $\phi_0 = h/|e|$. The occupied states for half filling are colored in blue. The Hall conductance values (in units of e^2/h) in some of the gaps are shown in red.

The spectrum for a ribbon geometry is shown in Fig. 6 for the same model, for a small magnetic flux. Figure 6 confirms the presence of edge states crossing the gap with the predicted chirality. An interesting difference between such a ribbon spectrum for a loop and that of a Hamiltonian with

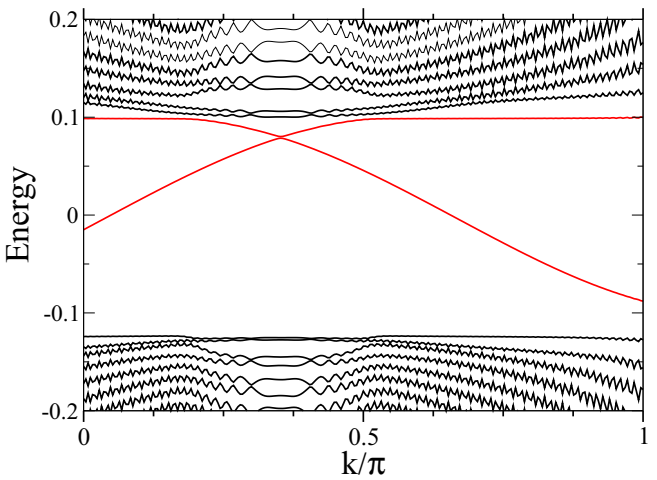

FIG. 6. Spectrum of model (11) for a ribbon geometry under a weak magnetic field flux $\phi/\phi_0 = 1/400$ vs longitudinal momentum. The edge states are highlighted in red.

two Dirac points [28] is readily apparent. In the latter, the LL's dispersion with longitudinal momentum is easily recognizable as plateaus, while in Fig. 6, such LL plateaus are not seen. The reason for this difference lies in the fact that LLs near the loop gap have high order, so that the wave functions ϕ_n in Eq. (15) contain high-order Hermite polynomials. The edge states, therefore, decay fairly slowly into the bulk, and finite-size effects (the ribbon's width) are relatively strong.

IV. CONCLUSION

We studied a minimal Dirac ring Hamiltonian with mass gap terms, for two-dimensional fermions, as a model for a Dirac loop anomalous Hall insulator. We derived an expression for the Chern number which assigns a chirality to the gapped loop through the phase winding of the mass gap terms. The change in the Chern number at a topological transition can also be calculated from a previously introduced index that we generalized to the Dirac loop case.

The Landau-level spectrum in a weak magnetic field was shown to depend on the loop's chirality. The Fermi level has a high LL index. In the case of an anomalous Hall insulator, a weak magnetic field turns the system into a metal, although it may become a trivial insulator at higher fields. In the spinful case of a topological insulator where spin s_z is conserved, the weak magnetic field's gauge field turns the system into a spin Hall insulator with finite magnetization.

We also studied the Hofstadter butterfly spectrum for arbitrary field, as well as the edge states in a ribbon geometry. The latter decay more slowly into the bulk and are therefore more sensitive to finite-size effects in the Dirac loop case when compared to the case of Dirac nodes.

A proposal for the realization of a Dirac loop semimetal in two dimensions has appeared recently [26]. We also expect that the models introduced above are suitable for realization in optical lattices.

[1] M. Z. Hasan and C. L. Kane, Rev. Mod. Phys. **82**, 3045 (2010).
[2] X. L. Qi and S. C. Zhang, Rev. Mod. Phys. **83**, 1057 (2011).
[3] A. Altland and M. R. Zirnbauer, Phys. Rev. B **55**, 1142 (1997); A. P. Schnyder, S. Ryu, A. Furusaki, and A. W. W. Ludwig, *ibid.* **78**, 195125 (2008); A. Kitaev, in *Periodic Table for Topological Insulators and Superconductors*, edited by V. Lebedev and M. Feigel'Man, AIP Conf. Proc. No. 1134 (AIP, New York, 2009), pp. 22–30.
[4] J. Alicea, Rep. Prog. Phys. **75**, 076501 (2012).
[5] X. Wan, A. M. Turner, A. Vishwanath, and S. Y. Savrasov, Phys. Rev. B **83**, 205101 (2011).
[6] P. Delplace, J. Li, and D. Carpentier, Europhys. Lett. **97**, 67004 (2012).
[7] J-.M. Hou, Phys. Rev. Lett. **111**, 130403 (2013).
[8] S. M. Young and C. L. Kane, Phys. Rev. Lett. **115**, 126803 (2015).
[9] S. Ganeshan and S. Das Sarma, Phys. Rev. B **91**, 125438 (2015).
[10] H. Nielsen and M. Ninomiya, Phys. Lett. B **130**, 389 (1983).
[11] Z. Wang, Y. Sun, X.-Q. Chen, C. Franchini, G. Xu, H. Weng, X. Dai, and Z. Fang, Phys. Rev. B **85**, 195320 (2012).
[12] S.-Y. Xu, C. Liu, S. K. Kushwadha, T.-R. Chang, J. W. Krizan, R. Shankar, C. M. Polley, J. Adell, T. Balasubramanian, K. Miyamoto. N. Alidoust, G. Bian, M. Neupane, I. Belopolski, H.-T. Jeng, C.-Y. Huang, W.-F. Tsai, H. Lin, F. C. CHou, T. Okuda, A. Okuda, A. Bansil, R. J. Cava, and M. Z. Hasan, arXiv:1312.7624.
[13] Z. K. Liu, B. Zhou, Y. Zhang, H. M. Weng, D. Prabhakaran, S.-K. Mo, Z. X. Shen, Z. Fang, X. Dai, Z. Hussain, and Y. L. Chen, Science **343**, 864 (2014).
[14] Z. Wang, H. Weng, Q. Wu, X. Dai, and Z. Fang, Phys. Rev. B **88**, 125427 (2013).
[15] Z. K. Liu, J. Jiang, B. Zhou, Z. J. Wang, Y. Zhang, H. M. Weng, D. Prabhakaran, S.-K. Mo, H. Peng, P. Dudin, T. kim, M. Hoech, Z. Fang, X. Dai, Z. X. Shen, D. L. Feng, Z. Hussain, and Y. L. Chen, Nat. Mater. **13**, 677 (2014).
[16] M. Neupane, S.-Y. Xu, R. Sankar, N. Alidoust, G. Bian, C. Liu, I. Belopolski, T.-R. Chang, H.-T. Jeng, H. Lin, A. Bansil, F. Chou, and M. Z. Hasan, Nat. Commun. **5**, 3786 (2014).
[17] S. Borisenko, Q. Gibson, D. Evtushinsky, V. Zabolotnyy, B. Büchner, and R. J. Cava, Phys. Rev. Lett. **113**, 027603 (2014).
[18] H. Weng, C. Fang, Z. Fang, B. A. Bernevig, and X. Dai, Phys. Rev. X **5**, 011029 (2015).
[19] S.-M. Huang, S.-Y. Xu, I. Belopolski, C.-C. Lee, G. Chang, B. Wang, N. Alidoust, G. Bian, M. Neupane, C. Zhang, S. Jia, A. Bansil, H. Lin, and M. Z. Hasan, Nat. Commun. **6**, 7373 (2015).
[20] S.-Y. Xu, I. Belopolski, N. Alidoust, M. Neupane, G. Bian, C. Zhang, R. Sankar, G. Chang, Z. Yuan, C.-C. Lee, S.-M. Huang, H. Zheng, J. Ma, D. S. Sanchez, B. Wang, A. Bansil, F. Chou, P. P. Shibayev, H. Lin, S. Jia, and M. Z. Hasan, Science **349**, 613 (2015).
[21] B. Q. Lv, H. M. Weng, B. B. Fu, X. P. Wang, H. Miao, J. Ma, P. Richard, X. C. Huang, L. X. Zhao, G. F. Chen, Z. Fang, X. Dai, T. Qian, and H. Ding, Phys. Rev. X **5**, 031013 (2015).
[22] L. X. Yang, Z. K. Liu, Y. Sun, H. Peng, H. F. Yang, T. Zhang, B. Zhou, Y. Zhang, Y. F. Guo, M. Rahn, D. Prabhakaran, Z. Hussain, S.-K. Mo, C. Felser, B. Yan, and Y. L. Chen, Nat. Phys. **11**, 728 (2015).
[23] K. Mullen, B. Uchoa, and D. T. Glatzhofer, Phys. Rev. Lett. **115**, 026403 (2015).
[24] R. Nandkishore, Phys. Rev. B **93**, 020506 (2016).
[25] Z. Yan and Z. Wang, Phys. Rev. Lett. **117**, 087402 (2016).
[26] J. L. Lu, W. Luo, X. Y. Li, S. Q. Yang, J. X. Cao, X. G. Gong, and H. J. Xiang, arXiv:1603.04596.
[27] M. V. Berry, Proc. R. Soc. London, Ser. A **392**, 45 (1984).
[28] M. A. N. Araújo and E. V. Castro, J. Phys. Condens. Matter **26**, 075501 (2014).
[29] H. B. Nielsen and M. Ninomiya, Nucl. Phys. B **185**, 20 (1981).
[30] L. Li and S. Chen, Phys. Rev. B **92**, 085118 (2015).
[31] T. Fukui, Y. Hatsugai, and H. Suzuki, J. Phys. Soc. Jpn. **74**, 1674 (2005).
[32] X. L. Qi, Y.-S. Wu, and S.-C. Zhang, Phys. Rev. B **74**, 085308 (2006).
[33] F. D. M. Haldane, Phys. Rev. Lett. **61**, 2015 (1988).

[34] N. Goldman, W. Beugeling, and C. Morais Smith, Europhys. Lett. **97**, 23003 (2012); Phys. Rev. B **86**, 075118 (2012).
[35] C. J. Tabert and E. J. Nicol, Phys. Rev. Lett. **110**, 197402 (2013).
[36] C. L. Kane and E. J. Mele, Phys. Rev. Lett. **95**, 146802 (2005).
[37] D. N. Sheng, Z. Y. Weng, L. Sheng, and F. D. M. Haldane, Phys. Rev. Lett. **97**, 036808 (2006).
[38] Xiao-Liang Qi, Yong-Shi Wu, and Shou-Cheng Zhang, Phys. Rev. B **74**, 045125 (2006).
[39] M. Onoda, Y. Avishai, and N. Nagaosa, Phys. Rev. Lett. **98**, 076802 (2007).
[40] D. R. Hofstadter, Phys. Rev. B **14**, 2239 (1976).
[41] S. Roy, M. Kolodrubetz, J. Moore, and A. Grushin, arXiv:1605.08445.